Michigan Technological University

Digital Commons @ Michigan Tech

Digital Commons @ Michigan Tech

Michigan Tech Publications

5-8-2018

Effect of Zr additions on thermal stability of Al-Cu precipitates in as-cast and cold worked samples

Kyle Deane
Michigan Technological University, kjdeane@mtu.edu

Paul G. Sanders
Michigan Technological University, sanders@mtu.edu

Follow this and additional works at: https://digitalcommons.mtu.edu/michigantech-p

Part of the Materials Science and Engineering Commons

Recommended Citation

Deane, K., & Sanders, P. G. (2018). Effect of Zr additions on thermal stability of Al-Cu precipitates in as-cast and cold worked samples. *Metals, 8*(5), 331. http://doi.org/10.3390/met8050331
Retrieved from: https://digitalcommons.mtu.edu/michigantech-p/1886

Follow this and additional works at: https://digitalcommons.mtu.edu/michigantech-p

Part of the Materials Science and Engineering Commons

metals

MDPI

Article

Effect of Zr Additions on Thermal Stability of Al-Cu Precipitates in As-Cast and Cold Worked Samples

Kyle Deane * and Paul Sanders

Materials Science Department, Michigan Technological University, Houghton, MI 49931, USA; sanders@mtu.edu
* Correspondence: kjdeane@mtu.edu; Tel.: +1-989-390-8150

Received: 9 April 2018; Accepted: 1 May 2018; Published: 8 May 2018

Abstract: While Zr is frequently added to Al alloys to control grain size with the formation of large (>1 μm) primary precipitates, little research has been conducted on the effect of nanoscale Al_3Zr precipitates on Al alloys. By comparing the precipitation and corresponding strength evolution between Al-Cu-Zr alloys with different Zr concentrations, the effects of Zr on Al-Cu precipitation with and without primary Al_3Zr precipitates can be observed. In the absence of these large precipitates, all Al_3Zr phases can be formed, through high temperature aging treatments, as a dispersion of nanoprecipaites inside the Al grains. In this study, Al-Cu-Zr ternary alloys were produced and heat treated to determine whether an increase in the coarsening resistance of Al-Cu precipitate phases would be observed with a distribution of the more thermally stable Al_3Zr nanoprecipitates. Generally, properly aged Al-Cu alloys will coarsen when encountering elevated temperatures higher than ~473 K (~200 °C). Diluted Al-Zr alloys (<0.07 at % Zr) resist coarsening behavior until the significantly higher temperatures of ~673 K (~400 °C), but are comparatively limited in strength because of a limited solubility of Zr in the Al matrix. Hardness testing and transmission electron microscope (TEM) results are discussed, in which it is found that even very small additions of Zr, when properly accounted for during heat treating, produce a finer microstructure and higher strength than in similar Al-Cu binary alloys. No significant change in the thermal stability of strengthening was observed, indicating that the finer precipitate microstructure is resultant from a higher nucleation density, as opposed to a decrease in coarsening behavior.

Keywords: aluminum; zirconium; precipitation strengthening; thermal stability

1. Introduction

Zirconium is an important alloying addition for aluminum alloys, mainly because of the thermal stability Al_3Zr phase in the Al matrix [1]. Al_3Zr precipitates are coarsening resistant up to temperatures greater than 673 K (400 °C) [1], which is ~200 K higher than commonly used precipitation strengthening additions in commercial alloys (Cu, Si, Mg, etc.). The low solubility of Zr in Al limits the effectiveness of Al_3Zr precipitates as a primary strengthening method [1,2], but this does not stop Zr from being widely researched and put to use in several key applications. The desirable thermal stability of Al_3Zr has led to Zr being added in hyperperitectic concentrations to numerous Al alloys to pin grain boundaries for use in superplastic deformation [1,2] and to refine grains in cold worked alloys [3,4]. It has been demonstrated as a complementary addition to the diluted Al-Sc alloy system for coherent nanoscale precipitation strengthening [5–7], and it is used in higher concentrations to form bulk metallic glass [8–10].

Throughout history, the majority of Al-Zr research has focused on alloys with Zr concentrations higher than the maximum solubility limit of Zr in the Al matrix phase, with the intent of forming large primary precipitates at the grain boundaries. The notable exception to this is the research focused on Al-Sc-Zr alloys, which relies on the absence of primary precipitates to achieve the maximum potential

precipitate strengthening for Al_3(Sc, Zr) precipitates. This work focuses on the interaction between Al-Cu and small Al-Zr precipitates, and thus does not require concentrations high enough to form primary Al_3Zr precipitates.

The primary goal of these experiments was to assess whether diluted Zr additions to Al-Cu alloys could increase the thermal stability of Al-Cu precipitation strengthening. If the refinement of microstructures associated with nanoscale Al_3Zr precipitates in Al-Cu alloys was shown to be partly because of a decrease in the coarsening kinetics of Al-Cu precipitates, it could be possible to increase the strength of more thermally stable Al alloys. To examine this effect, two sets of experiments were run, each comparing Al-Cu and Al-Cu-Zr alloys: (1) an isothermal heat treatment at 473 K (200 °C), quenching and taking hardness measurements periodically throughout the hold; and (2) a multi-step heat treatment that increased in temperature from 443 K (170 °C) to 643 K (370 °C) with five hour holds at each temperature, quenching and taking hardness measurements between each step.

As the goal of these experiments was to observe the effect of Al_3Zr nanoprecipitates on Al-Cu precipitation, two different concentrations of Zr were observed: 0.05 at % Zr (primary precipitate free) and 0.2 at % (primary precipitate forming). It was necessary to nucleate and grow the desired nanoprecipitates with an initial heat treatment procedure before holding at 443 K (170 °C). Relevant phase diagrams were consulted to determine appropriate heat treatments for these alloys, with the end goal of having the majority of Zr solute atoms precipitated out of solution into coherent Al_3Zr nanoprecipitates, while retaining the Cu solute atoms in solution in the matrix. The concentration levels of Zr and Cu in these alloys are low enough that the respective binary phase diagrams can approximate the trends expected in the ternary alloy. These phase diagrams (Figure 1), along with the listed points that immediately follow this paragraph, describe the heat treatment steps that were decided on and the reasoning behind their selection.

1. The first required heat treatment step was designed to nucleate Al_3Zr nanoprecipitates. The literature review indicates that precipitation strengthening behavior occurs in Al-Zr alloys at and above ~648 K (375 °C) [5,6]. The ideal temperature for this step was taken to be at the low end of the range, 648 K (375 °C), to reduce the final size of the Al_3Zr precipitates. This goal was made more challenging by the requirements of the second step.
2. As the temperature of the first step was sufficiently high enough to fully precipitate and anneal Al-Cu precipitates, the second required step was designed to re-solutionize the Cu solute atoms, such that preferred microstructural arrangements and strengthening could be achieved at a later step. To reduce overaging of the Al_3Zr precipitates, it was desired to keep this step as low in temperature as possible while still achieving solutionization of Cu. With this in mind, 773 K (500 °C) was chosen.
3. Once the initial heat treatment steps were completed and the microstructure was created, the aging and overaging steps were performed, as discussed in Section 2. Aging steps were selected to be below 473 K (200 °C), closely approximating the artificial aging treatments of binary Al-Cu alloys.

Looking at the phase diagrams in Figure 1 [11,12], several other notable conclusions about the proposed processing can be drawn. For one, the high liquidus temperature range of the Al-Zr phase diagram makes it necessary to reach much higher temperatures with the melting of Zr bearing alloys in order to fully dissolve Al_3Zr precipitates into the liquid. This effect is even more pronounced when adding Zr from master alloys with higher comparative Zr contents, as the large Zr precipitates sink and can create regions of the melt with disproportionately high liquidus temperatures.

Another notable conclusion is that it will be impossible to solutionize the Zr once these alloys are created. The relevant temperatures for solutionizing Zr are well above those necessary to begin melting in the Al-Cu system. Therefore, proper care must be taken with these alloys, as they are less forgiving of failed heat treatments than current precipitation strengthening alloys.

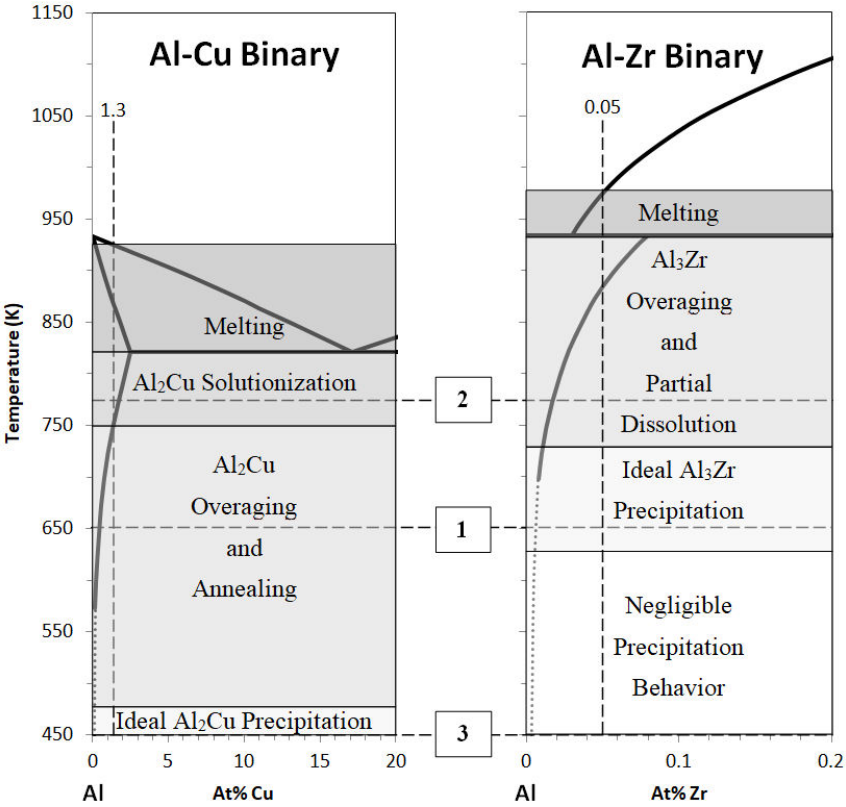

Figure 1. These phase diagrams [11,12] demonstrate the challenge of choosing optimal heat treatments for Al-Cu-Zr alloys. As these alloys have very low Zr content, the binary diagrams are relevant enough approximations to the ternary reality to assist in determining trends. Vertical dashed lines on these diagrams denote the main alloy used in this study. The horizontal dashed lines (1, 2, and 3) indicate the order/temperature of heat treatment steps required to nucleate and grow Al_3Zr precipitates before aging. The list preceding this image in Section 1 describes these steps more fully.

Finally, it can be noted that at the Al-Cu solutionizing temperature of 773 K (500 °C), Al_3Zr precipitates have been observed to partially dissolve into the solid solution because of an increased solubility of Zr in Al, indicated in the literature by a decrease in electrical conductivity after undergoing heat treatments at elevated temperatures [5,6]. This dissolution behavior is not ideal, but it also cannot be reasonably avoided. The Al-Cu solutionizing temperature can in fact be lowered to a temperature that would better preserve the Al_3Zr precipitates, but the only way to achieve this in this ternary system is to decrease the alloy Cu concentration, and in turn the potential for Al-Cu strengthening (see the solvus line for the Al-Cu binary in Figure 1).

2. Materials and Methods

In preparation for casting the new alloys, master alloys were cut up using a band saw, cleaned thoroughly using an ultrasonic bath with acetone, and weighed out in the proper amounts to make ~600 g charges of the compositions listed in Table 1. The resulting charges were then cast in a vacuum induction melter (VIM, constructed at Michigan Technological University, Houghton, MI, USA) into a bottom-fed permanent mold to create cylindrical bars approximately 19mm in diameter. After evacuation of the chamber, the charges were held in a liquid state at 1173 K (900 °C) for 10 min under a 99.999% purity argon atmosphere at ~684 torr. After solidification, samples with a thickness of ~1 cm were sectioned from the center of one cylindrical bar from each casting using an abrasive cutoff disc, and mounted in QuickSet epoxy. The mounted samples were then ground and polished to a final finishing step of 0.04 micron colloidal silica.

Table 1. Expected and Observed Alloy Compositions.

Element	Al-1.3 at % Cu		Al-1.3 at % Cu-0.05 at % Zr		Al-1.3 at % Cu-0.25 at % Zr	
	Target	ICP	Target	ICP	Target	ICP
Cu (at %)	1.30	1.30	1.30	1.42	1.30	1.31
Zr (at %)	-	-	0.05	0.05	0.25	0.27

A hole was also drilled in each casting to create chips that could be dissolved for ICP-OES analysis. For each sample, approximately 0.4 g of these chips was dissolved in HCl and HNO_3 using an Anton Paar microwave digestion setup, followed by dilution with water into a final solution volume of 100 mL. ICP-OES was performed with a Perkin Elmer Optima 7000DV to verify the Cu and Zr concentrations for each casting. Typical detection limits for ICP-OES on this machine, according to Perkin Elmer documentation, range between 0.15 and 4.5 µg/L for reported elements. Coincidentally, both Al and Cu have the same reported detection limit of 0.9 µg/L. The detection limit of Zr is not reported, thus it was estimated here to match the highest reported detection limit of 4.5 µg/L. As each sample consisted of 0.4 g of alloy dissolved and diluted into a 100 mL solution, these detection limits correspond to minimum detectable alloy concentrations of 2.25×10^{-4} wt % for Al and Cu and 1.125×10^{-3} wt % for Zr, which are well below the alloy concentrations used in this study.

Vickers hardness testing was performed for each sample using a LECO MHT Series 200 hardness tester (LECO Corporation, St. Joseph, MI, USA). Using the automated XY stage, hardness indents were created with 10 g of force and a 15 s hold time in a large grid across the sample. For the isothermal aging study (Table 2), indents were performed in a 2×5 grid for a total of 10 points, and for the stepped aging study (Table 2), indents were performed in a 3×10 grid for a total of 30 points. The hardness data reported in Section 3 represent the average value of one grid of hardness indents (10 or 30 points, depending on the study), with error bars indicating the 95% confidence interval within the hardness grid.

Table 2. Heat Treatment Schedules for Al-Cu-Zr Experiments.

Step	Step Intent	Isothermal Aging at 473 K		Stepped Aging	
		Time (h)	Temp (K)	Time (h)	Temp (K)
(1)	Nucleate Al_3Zr	3	623	3	648
(2)	Solutionize Cu	3	798	1	773
(3)	Age	6	473	5	443
(4)	↓	12 (18 total)	473	5	493
(5)	Over-age	18 (36 total)	473	5	543
(6)	↓	24 (60 total)	473	5	593
(7)	↓	30 (90 total)	473	5	643
(8)	↓	36 (126 total)	473	-	-
(9)	↓	42 (168 total)	473	-	-
(10)	↓	48 (216 total)	473	-	-

After evaluating these indents, the epoxy was broken off of the sample in preparation for heat treatment using a bench-mounted vice, taking care not to deform the relatively soft aluminum sample. Heat treatment was performed on the samples in a Thermolyne box furnace with a Furnatrol 53,600 Controller, according to the schedules depicted in Table 2. Between each heat treatment step, the samples were quenched in water as they were removed, and epoxy was then re-applied to the samples in such a way that minimal polishing was required to achieve a freshly polished surface. Another round of 30 hardness tests were performed, offset from the previous indent grids to avoid unwanted interactions, and then the sample was again broken out of the epoxy and placed back in the furnace at the next temperature. This process (mount → hardness test → unmount → heat treat → repeat) was repeated until all heat treatment steps were complete.

After completion of the stepped aging heat treatment described in Table 2, transmission electron microscope (TEM) samples were created from each of the specimens. TEM sample preparation was performed as follows: 0.5 mm thick slices were cut from the sample using a Japax Lux3 Wire EDM (Japax, Japan). Each slice was then polished on both sides to a mirror surface, and 3 mm diameter discs were punched out using a specialized hole punch. Using a Gatan Disc Grinder system, these discs were polished further on each side to yield a final thickness of approximately 50 microns, and a final surface polished with 0.04 micron colloidal silica. These discs were then perforated with a Metalthin Twin Jet Electropolishing System (South Bay Technology Inc., San Clemente, CA, USA), using a solution of 29% reagent grade nitric acid and 71% reagent grade methanol. The solution was kept below 243 K (−30 °C) with a Multicool recirculating methanol refrigeration unit. The relevant operating settings for the Metalthin instrument were as follows: 20–30 volts, jet speed of 4, sensitivity of 7–8.

Successfully prepared TEM specimens were analyzed on a JEOL JEM-2010 high resolution transmission electron microscope (JEOL, Tokyo, Japan). All images were captured with a Gatan Orius SC200 high-speed digital camera, and chemical analysis of nanoscale features was performed using an Oxford energy dispersive spectrometer (EDS). TEM analysis of these specimens yielded images of hundreds of precipitates for each heat treated specimen. The length and width of all resolvable precipitates were measured manually using the freely available image processing software ImageJ.

3. Results and Discussion

Figures 2 and 3 describe the strengthening behavior observed for the isothermal and stepped aging experiments, respectively. From these results, it could immediately be seen that all Zr-bearing Al-Cu alloys invariably maintained a higher strength than the binary Al-Cu alloys, by what appears to be a constant strengthening increment for each set of experimental parameters. This strengthening increment appears to be thermally stable at elevated temperatures that would normally coarsen and overage Al-Cu (primarily Al_2Cu) precipitates. This information taken by itself was promising, especially considering that the alloy containing only 0.05 at % Zr was shown to have a similar strengthening effect as the alloy containing 0.2 at % Zr, implying that aged, nanoscale Al_3Zr precipitates are equally as effective as the larger primary precipitates. However, the results did not indicate any noticeable increase in thermal stability of the total precipitation strengthening that would be expected to accompany any improvement in coarsening resistance of the Al-Cu precipitate phases.

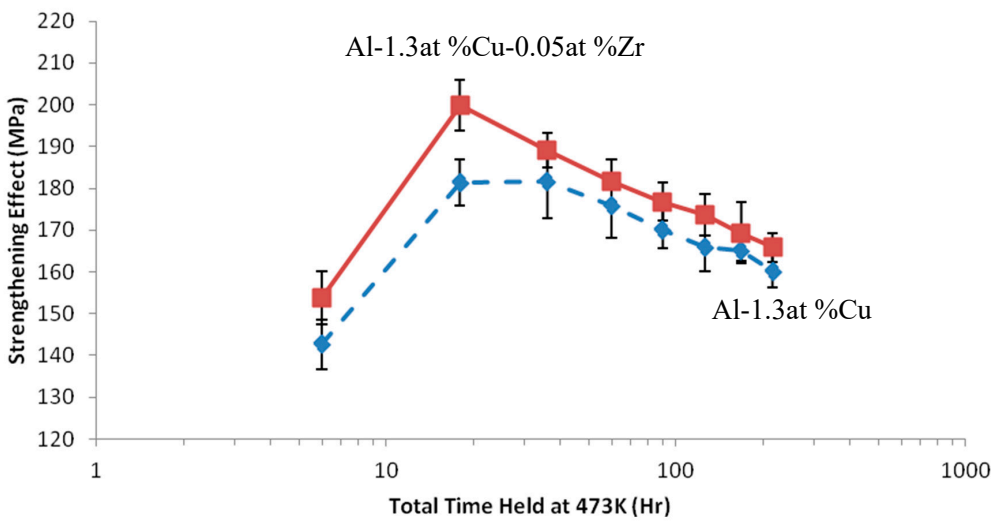

Figure 2. This plot describes the overaging of two Al-Cu alloys at 473 K (Table 2 isothermal), one alloy with Zr additions and one without. In this experiment, the Zr-containing alloy consistently had a slightly higher strengthening than the Al-Cu binary. Error bars represent a 95% confidence level in the mean hardness data (10 Vickers indents in a grid across the sample for each point).

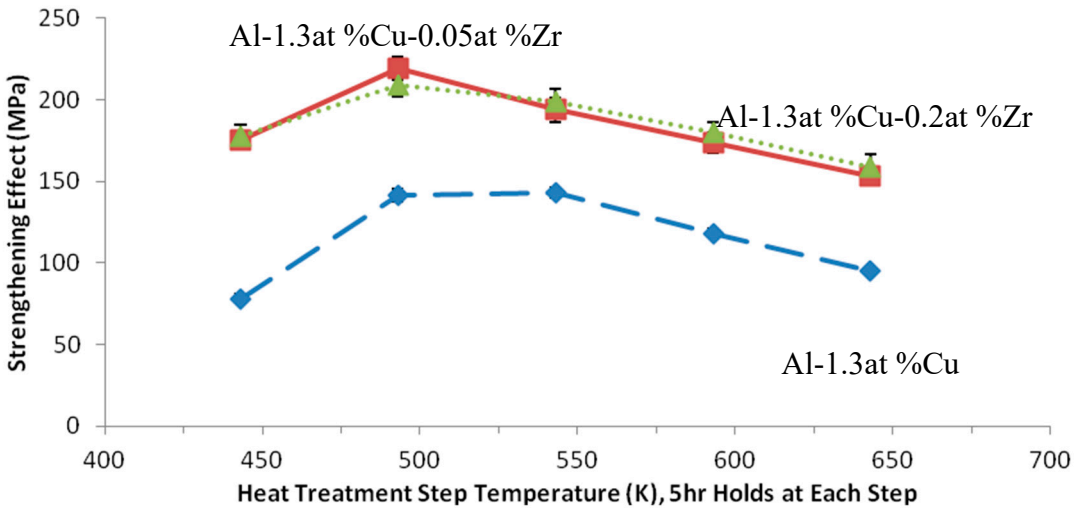

Figure 3. This plot describes the overaging of Al-1.3 at % Cu as consecutively higher 5 hr heat treatments were performed (Table 2 stepped), compared with overaging in the same alloy with two different levels of Zr additions. While there is little statistical difference between the two Zr-bearing alloys, a significant higher strengthening effect can be observed in both of them when compared with the Al-Cu binary. Error bars represent a 95% confidence level in the mean hardness data (30 Vickers indents in a grid across the sample for each point).

Without consulting TEM images of the sample microstructure, the false assumption could be reached that the Zr additions do not significantly affect the Al-Cu precipitation behavior, and that the observed thermally stable strengthening increment is entirely because of strengthening contributions of Al_3Zr nanoprecipitates. However, TEM images of the samples taken after completion of stepped aging (Table 2) negate this possibility. In these images, Al-Cu precipitates found in the Al-1.3 at % Cu sample have measured lengths ~3× longer than the precipitates found in both of the Al-1.3 at % Cu-(0.05, 0.2) at % Zr samples, suggesting that the addition of Zr does significantly affect the precipitation behavior of Al-Cu precipitates. Representative images are shown in Figure 4.

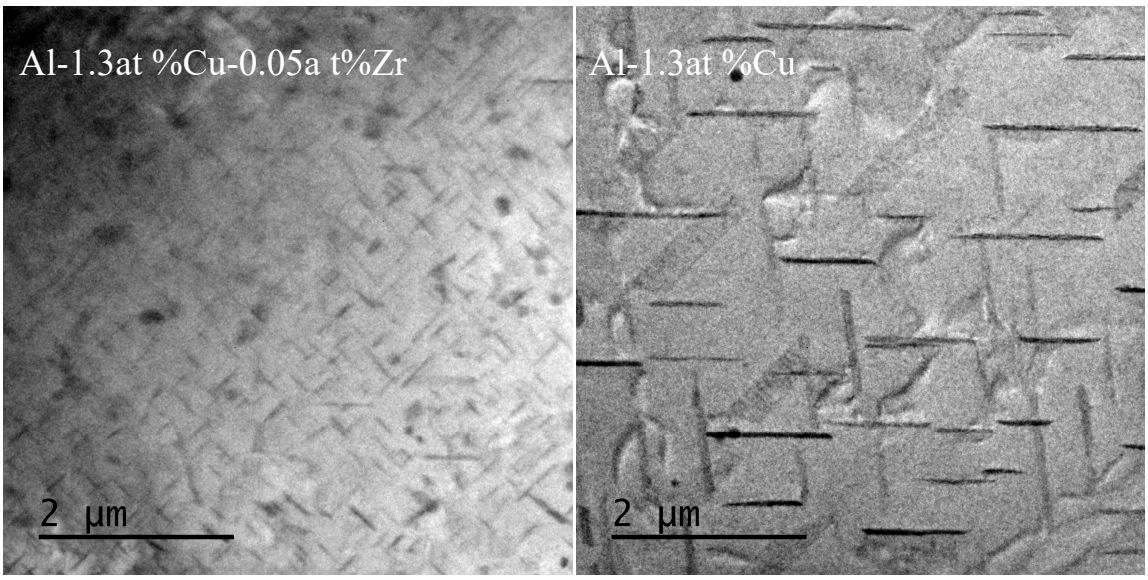

Figure 4. These TEM images, taken after completion of the 643 K (370 °C) stepped heat treatment described in Section 2, demonstrate the difference in Al-Cu precipitate growth between an Al-Cu alloy with and without Zr additions.

A comparison of observed precipitate lengths and aspect ratios between the three alloys that underwent the stepped aging heat treatment (Table 2) can be seen in Figure 5. This comparison indicates that the Al-Cu precipitate aspect ratio distributions are consistent between Al-Cu and Al-Cu-Zr alloys. It also shows that the average Al-Cu precipitate length, while similar in both observed Al-Cu-Zr alloys, is noticeably larger in the binary Al-Cu alloy.

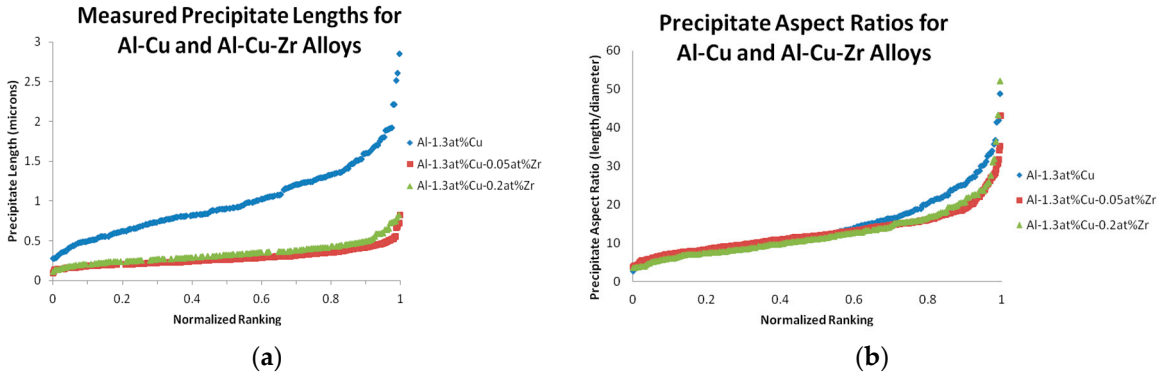

Figure 5. These graphs show the observed (**a**) lengths and (**b**) length/width aspect ratios of Al-Cu (primarily Al_2Cu) precipitates in the three different alloys. These measurements were made on TEM images of the alloys after completion of the 643 K (370 °C) stepped aging heat treatment (Table 2).

Orowan strengthening contributions of the oblong θ′ precipitates can be estimated using Equation (1) [13], where M = 3.06 is the Taylor factor [14], G = 25.4 GPa is the shear modulus of the matrix [15], b = 0.286 nm is the Burgers vector magnitude of the matrix [15], and r_0 = 0.572 nm is the inner dislocation cut-off radius [16]. Image analysis of the TEM images yields average precipitate plate diameter (D_p) and an estimate of the thickness (t_p), although the actual thickness can be assumed to be slightly lower than this estimate because of unknown disorientation of the TEM images. The volume fraction (f_v) can be assumed to be at equilibrium and estimated from the solvus composition for a given alloy.

$$\sigma_{\theta'} = 0.13MG\frac{b}{(D_p t_p)^{1/2}}\left[f_v^{1/2} + 0.75(D_p/t_p)^{1/2} f_v + 0.14(D_p/t_p) f_v^{3/2}\right]\cdot ln\left(\frac{0.87(D_p t_p)^{1/2}}{r_0}\right) \quad (1)$$

Using this method, Orowan strengthening contributions of the θ′ precipitates were estimated to be 23.9 and 63.9 MPa for Al-1.3 at % Cu and Al-1.3 at % Cu-0.05 at % Zr alloys, respectively, after the final stepped heat treatment step of 643 K (370 °C). The difference between these two estimates is ~40 MPa, which accounts for a significant amount of the observed difference between these alloys of ~58 MPa.

Upon closer inspection of the TEM samples for the Al-Cu-Zr alloys, a fine dispersion of rounded Zr-rich nanoprecipitates becomes apparent among the larger θ′ precipitates, as seen in Figure 6. When analyzed with EDS, these rounded precipitates contain not only Al and Zr, as would be expected with simple Al_3Zr precipitate phase, but significant quantities of Cu as well, when compared with the matrix (Figure 7).

The formation of these Zr-rich precipitates could only have occurred during the initial heat treatment step, which was intended to solutionize Cu and simultaneously form the Al_3Zr phase. It is unclear whether this phenomenon is because of an attraction of Cu atoms to the stable Al_3Zr precipitates at these higher temperatures, or to the formation of a stable, ternary Al-Cu-Zr phase. While many Al-Cu-Zr intermetallic phases are known to exist, only the τ_9 phase (Al-15.7 at % Cu-17.1 at % Zr) is predicted to potentially be stable with the given alloy composition at 773 K (500 °C) [8,17].

One consequence of forming Al-Cu-Zr precipitates, as opposed to the simple Al_3Zr phase, is that a small amount of Cu is depleted from the matrix and made unavailable for θ′ precipitates. However, assuming all Zr matrix content is used to form τ_9 precipitates, the maximum loss in matrix Cu content would still only be ~0.046 at % Cu for the Al-1.3 at % Cu-0.05 at % Zr alloy and ~0.072 at % Cu for the Al-1.3 at % Cu-0.2 at % Zr alloy (assuming a Zr solubility limit of 0.078 at % Zr). This is expected to result in a decrease in the final θ′ precipitate phase fraction of up to ~5% when compared with the Al-1.3 at % Cu binary alloy.

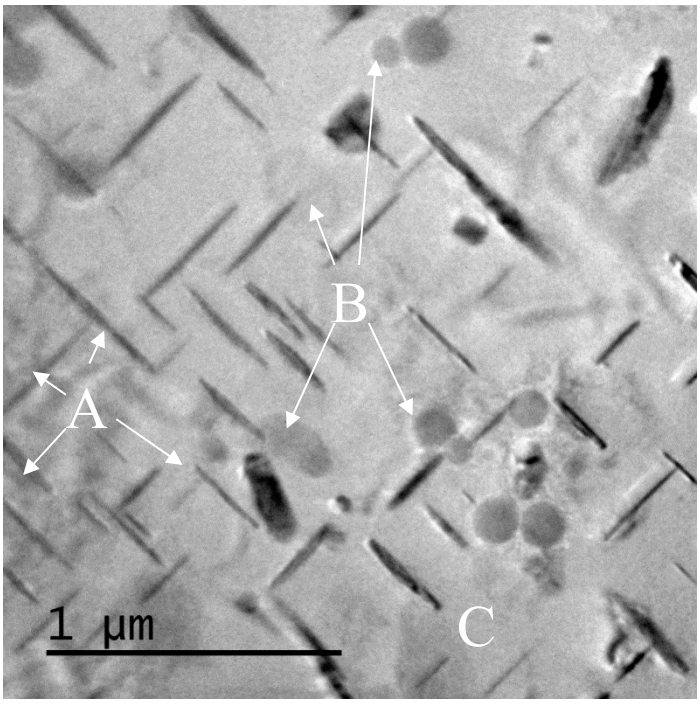

Figure 6. This TEM image of the Al-1.3 at % Cu-0.05 at % Zr sample, taken after completion of the 643 K (370 °C) stepped heat treatment described in Section 2, shows the three different phases observed during TEM of the Al-Cu-Zr alloys: (**A**) elongated θ′ precipitates; (**B**) rounded Zr-rich precipitates; and (**C**) the Al matrix phase. Several locations where θ′ precipitates and the Zr-rich precipitates intersect are visible within this image as well.

It is also interesting to note that the θ′ and Zr-rich precipitates intercept each other in several instances within Figure 6. These instances are representative of all such behavior observed in other Al-Cu-Zr TEM images, in that the elongated θ′ precipitates tend to terminate in or on a Zr-rich precipitate when they intercept. This behavior may be indicative of the nucleation of θ′ precipitates on the previously formed Zr-rich precipitates [17]. Nucleation on Al_3Zr precipitates could account for the Cu-enriched nature of the Zr-rich phase. This nucleation phenomenon contributes to an increased number density of θ′ precipitates, which in turn results in lower average dimensions of θ′ precipitates in the Zr-bearing alloys when compared with the binary alloys.

Comparison of TEM EDS scans for the three phases indicated in Figure 6 can be found in Figure 7. The difference in Cu:Zr intensity ratios between the θ′ and τ_9 precipitates in Figure 7 clearly indicates that the two precipitate phases are of different compositional makeup. It should also be noted that the Zr content in the scan for the θ′ precipitate is not universal; some of the θ′ precipitates observed showed no noticeable Zr content, while others still showed Zr quantities between the matrix and Al_3Zr concentrations. This discrepancy could potentially be due to inaccuracies in measuring low concentration elements in relatively thin precipitates, or to the unknowing contamination of signal from small, nearby Zr-rich precipitates.

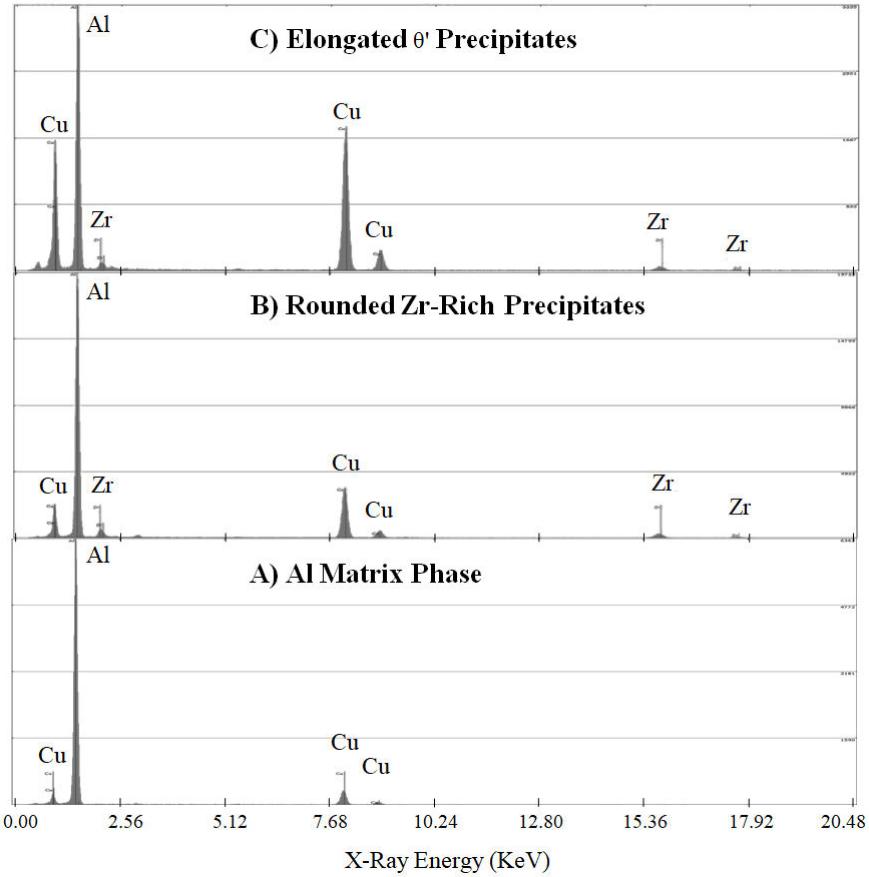

Figure 7. During TEM analysis of Al-1.3 at % Cu-0.05 at % Zr samples aged according to the schedule for Experiment 2 (Table 2), these energy dispersive spectrometer (EDS) scans were obtained of the three main phases that were observed. Microstructural images of these phases, labeled as **A**, **B**, and **C**, are clearly pointed out in Figure 6.

4. Conclusions

In this research, experiments were run to determine whether Al_3Zr nanoprecipitates, formed with a custom heat treatment and diluted Zr additions to Al-Cu binary alloys, could increase the thermal stability of the relevant Al-Cu precipitates. Different alloy compositions were observed in order to differentiate between the effect of large primary Al_3Zr precipitates and the aged nanoprecipitates. While no significant change in the rate at which strengthening decreased during overaging was observed, TEM images taken at the end of overaging heat treatments clearly depict θ′ precipitates in the binary alloys achieving dimensions approximately three times larger than in the Al-Cu-Zr ternary alloys. Also present in TEM images of the Al-Cu-Zr alloys were rounded nanoprecipitates that were found to contain both Zr and Cu atoms at higher levels than the matrix concentration. These precipitates are believed to be either Cu-enriched Al_3Zr phase or τ_9 phase, which has a composition of Al-15.7 at % Cu-17.1 at % Zr and has been reported to be stable with the alloy concentration at the initial Al-Zr aging step of 773 K (500 °C) [8,17]. It is indicated, from the positioning of the θ′ relative to the Zr-rich precipitates, that the latter precipitates appear to behave as nucleation sites for the Al-Cu precipitates, increasing the nucleation density and limited average growth of the θ′ precipitates.

The difference in strengths between the binary and ternary alloys can be mostly accounted for as the difference in Orowan strengthening because of the difference in precipitate dimensions and phase fractions. Image analysis of the precipitates provided enough data to estimate Orowan strengthening of the precipitates in the binary and ternary alloys, and the estimated difference of ~40 MPa explains

the majority of the observed difference in strengthening of ~58 MPa. Further differences in the strengthening are likely to be a combination of error in the strengthening calculations and the added strengthening benefit of the Zr-rich precipitates. It should also be noted that a large fraction of the strengthening of these alloys is due to solid solution strengthening, which behaves similarly in both alloys and is significant because of the relatively high solubility of Cu in the Al matrix. However, the strengthening effect of the precipitates is still a significant factor, and differences in the coarsening behavior, if present, should be reflected in the total strength. The fact that little difference in the thermal stability of strengthening was observed appears to imply that the coarsening rate is not significantly different with the addition of Zr (in either concentration), but that there were simply higher initial precipitate nucleation events in the Al-Cu-Zr alloys due to the presence of the aged Al_3Zr nanoprecipitates. Therefore, the average precipitate size was smaller in Zr bearing alloys by the time precipitate growth transitioned from being mainly matrix-depletion driven to being coarsening driven.

Future experiments should attempt to more thoroughly document Al-Cu precipitate growth with TEM throughout overaging in an attempt to understand this phenomenon more fully, as this study only had access to TEM images after aging was completed. Collecting TEM precipitate size distributions concurrently with the strengthening data taken between each heat treatment step would allow insight into how strengthening sources evolve differently with and without the presence of Zr. TEM images from earlier in the aging process may also confirm the proposal that nucleation of Al-Cu precipitates was assisted by the presence of Al_3Zr nanoprecipitates, causing the initial strengthening differences. The proposed experiments should include long isochronal aging of Al-Cu-Zr alloys with an initial high temperature aging step to nucleate Al_3Zr/τ_9 nanoprecipitates, as described in this study.

Author Contributions: K.D. and P.S. conceived and designed the experiments; K.D. performed the experiments; K.D. and P.S. analyzed the data; K.D. wrote the paper; P.S. proofread and edited the paper.

Acknowledgments: This work was funded by the Office of Naval Research, grant No. N00014-11-10876.

Conflicts of Interest: The founding sponsors had no role in the design of the study; in the collection, analyses, or interpretation of data; in the writing of the manuscript, and in the decision to publish the results. The authors declare no conflict of interest.

References

1. Padmanabhan, K.A.; Davies, G.J. *Superplasticity: Mechanical and Structural Aspects, Environmental Effects, Fundamentals and Applications*; Springer Science & Business Media: Berlin, Germany, 2012.
2. McNelley, T.R.; McMahon, M.E.; Pérez-Prado, M.T. Grain boundary evolution and continuous recrystallization of a superplastic Al-Cu-Zr alloy. *Philos. Trans. R. Soc. Lond. Math. Phys. Eng. Sci.* **1999**, *357*, 1683–1705. [CrossRef]
3. Liu, J.; Yao, P.; Zhao, N.; Shi, C.; Li, H.; Li, X.; Xi, D.; Yang, S. Effect of minor Sc and Zr on recrystallization behavior and mechanical properties of novel Al-Zn-Mg-Cu alloys. *J. Alloys Compd.* **2016**, *657*, 717–725. [CrossRef]
4. Wang, Y.; Pan, Q.; Song, Y.; Li, C.; Li, Z.; Chen, Q.; Yin, Z. Recrystalization of Al-5.8Mg-Mn-Sc-Zr alloy. *Trans. Nonferrous Met. Soc. China* **2013**, *23*, 3235–3241. [CrossRef]
5. Knipling, K.E.; Karnesky, R.A.; Lee, C.P.; Dunand, D.C.; Seidman, D.N. Precipitation evolution in Al-0.1 Sc, Al-0.1 Zr and Al-0.1 Sc-0.1 Zr (at %) alloys during isochronal aging. *Acta Mater.* **2010**, *58*, 5184–5195. [CrossRef]
6. Knipling, K.E.; Seidman, D.N.; Dunand, D.C. Ambient-and high-temperature mechanical properties of isochronally aged Al-0.06 Sc, Al-0.06 Zr and Al-0.06 Sc-0.06 Zr (at %) alloys. *Acta Mater.* **2011**, *59*, 943–954. [CrossRef]
7. Fuller, C.B.; Seidman, D.N.; Dunand, D.C. Mechanical properties of Al (Sc, Zr) alloys at ambient and elevated temperatures. *Acta Mater.* **2003**, *51*, 4803–4814. [CrossRef]
8. Bo, H.; Wang, J.; Jin, S.; Qi, H.Y.; Yuan, X.L.; Liu, L.B.; Jin, Z.P. Thermodynamic analysis of the Al-Cu-Zr bulk metallic glass system. *Intermetallics* **2010**, *18*, 2322–2327. [CrossRef]
9. Jiang, Q.K.; Wang, X.D.; Nie, X.P.; Zhang, G.Q.; Ma, H.; Fecht, H.-J.; Bendnarcik, J.; Franz, H.; Liu, Y.G.; Cao, Q.P.; et al. Zr-(Cu, Ag)-Al bulk metallic glasses. *Acta Mater.* **2008**, *56*, 1785–1796. [CrossRef]

10. Sun, Y.J.; Qu, D.D.; Huang, Y.J.; Liss, K.-D.; Wei, X.S.; Xing, D.W.; Shen, J. Zr-Cu-Ni-Al bulk metallic glasses with superhigh glass-forming ability. *Acta Mater.* **2009**, *57*, 1290–1299. [CrossRef]
11. Murray, J.L. The aluminium-copper system. *Int. Met. Rev.* **1985**, *30*, 211–234. [CrossRef]
12. Zhu, A.W.; Chen, J.; Starke, E.A. Precipitation strengthening of stress-aged Al-xCu alloys. *Acta Mater.* **2000**, *9*, 2239–2246. [CrossRef]
13. Meyers, M. *Mechanical Metallurgy: Principles and Application*, 1st ed.; Prentice-Hall, Inc.: Englewood Cliffs, NJ, USA, 1983.
14. Fukunaga, K.; Shouji, T.; Miura, Y. Temperature dependence of dislocation structure of L12-Al3Sc. *Mater. Sci. Eng. A* **1997**, *239*, 202–205. [CrossRef]
15. Kelly, P.M. The effect of particle shape on dispersion hardening. *Scr. Metall.* **1972**, *6*, 647–656. [CrossRef]
16. M.S.I.T. Msit®. *Light Metal Systems*; Part 2; Effenberg, G., Ilyenko, S., Eds.; Springer: Berlin/Heidelberg, Germany, 2005; pp. 1–17.
17. Kanno, M.; Ou, B.-L. Heterogeneous Precipitation of Intermediate Phases on Al3Zr Particles in Al-Cu-Zr and Al-Li-Cu-Zr Alloys. *Mater. Trans. JIM* **1991**, *32*, 445–450. [CrossRef]

© 2018 by the authors. Licensee MDPI, Basel, Switzerland. This article is an open access article distributed under the terms and conditions of the Creative Commons Attribution (CC BY) license (http://creativecommons.org/licenses/by/4.0/).